

IN-FLIGHT EXPERIMENTS FOR DELAYING LAMINAR-TURBULENT TRANSITION ON A LAMINAR WING GLOVE

Inken Peltzer, Andreas Pätzold, Wolfgang Nitsche
Chair for Aerodynamics

Department of Aeronautics and Astronautics

Berlin Institute of Technology

Marchstr. 12, 10587 Berlin, Germany

phone: +49 30 314 23094

fax: +49 30 314 22955

e-mail: Inken.Peltzer@tu-berlin.de

Keywords: *Active Flow Control, Laminar-Turbulent Transition, Damping of Tollmien-Schlichting Instabilities, In-flight Measurements*

Abstract

This paper describes in-flight measurements to delay laminar-turbulent transition by means of active Tollmien-Schlichting (TS) wave cancellation. It is a well known fact that the damping or cancellation of unstable TS-waves in the boundary layer leads to downstream shifting of the laminar-turbulent transition and therefore to the reduction of skin friction. In-flight experiments were carried out using a laminar wing glove for a sailplane. A sensor-actuator system attached to the wing glove consisted of an array of surface hot-wire reference sensors to detect oncoming TS-waves upstream of a membrane actuator and surface hot-wire error sensors downstream of the actuator. The method applied to delay laminar-turbulent transition is based on the damping of naturally occurring instabilities through superimposition of the counter wave, which is calculated by a fast digital signal processor (DSP) using a closed loop feed-forward control algorithm. The actuator signal is calculated directly from this signal using a linear transfer function (finite impulse response, FIR). The FIR-filter models the amplification and the propagation of TS-waves in the linear stage. Subsequently, an amplified, phase-shifted anti-wave is calculated from the

DSP and introduced into the boundary layer. The error sensor measures the remaining disturbances downstream of the actuator and feeds them into the control-system. The experiments were carried out at flight velocities in the region of 20m/s, which corresponds to a chord Reynolds number of about 2 million. The results show a damping of 10dB or a 60% reduction of the local amplitudes of the instabilities. This illustrates the potential of this method for applications in atmospheric conditions experienced in-flight. It is anticipated that using an actuator with a high resonance frequency and a minimal reaction time will improve damping significantly in future experiments.

1 Nomenclature

f	frequency
Re_c	Reynolds number based on the chord
t	time
t_a	response time of the actuator
u_∞	freestream velocity
U	voltage
x/c	normalised chord
AWC	Active Wave Control
DSP	Digital Signal Processor
LMS	Least Mean Square
RMS	Root Mean Square
TS	Tollmien-Schlichting

2 General Introduction

Drag reduction by delaying laminar-turbulent transition is one of the main goals in today's aerodynamic research. Many active and passive methods have been investigated in this field [8, 2, 1]. One active method is the cancellation of Tollmien-Schlichting (TS) instabilities by superimposing them with proper anti-waves, which was extensively investigated in a wind tunnel. The basic investigations by Milling [12] and by Liepmann et al. [11] have shown the possibility to attenuate TS-waves. These experiments were carried out primarily using artificial disturbances. A large number of experimental and numerical investigations dedicated to this topic followed [9, 14, 4, 10, 7]. Thomas [18] worked in the same field and was most likely the first to realize the problem around the random occurrence of the broadband natural TS-waves. Experiments to actively control natural TS-instabilities were less frequent [17, 6]. Since the growth of TS-instabilities strongly depends on environmental flow conditions, it is necessary to investigate the transition under real flight conditions [15]. Therefore the investigations presented in this paper are aimed at measurements of TS-instabilities and their cancellation in flight experiments.

Natural TS-wave packets occur randomly. Therefore, a high attenuation can only be achieved by a closed loop feed-forward control algorithm. A fast digital signal processor (DSP) was required to ensure optimal active wave control (AWC). In addition, sensors detecting the disturbances and actuators introducing counter waves were required and integrated into the wing surface to avoid any further roughness. A principle sketch of this approach is shown in Fig.1.

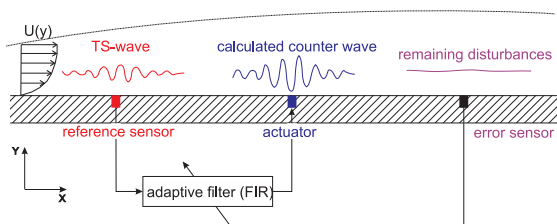


Fig. 1 Principle of the active wave control

The actuator signal was calculated directly from the measured signal of the reference sensor via a convolution with a linear transfer function (finite impulse response, FIR). The transfer function is continuously adapted to ensure that the error signal, measured downstream of the actuator, can be minimized using the least mean square (LMS) algorithm. This method of active wave control is derived from a control method which was initially used in the field of active noise control [5].

3 Experimental Setup

A Grob G103 TWIN II two-seater sailplane (Fig.2) at the Institute for Aeronautics and Astronautics at the Berlin Institute of Technology, was used for the in-flight experiments. The glove (Fig.3) is mounted on the right wing between the air brakes and the ailerons.

The measuring glove has a 2D central section with a 1.0m span and a chord length of 1.22m that includes the removable measurement section. Furthermore it has an exchangeable wing segment with a 0.6m span to be able to be utilized in different measuring tasks and objectives. The measuring equipment, such as the constant temperature anemometer, charge and voltage amplifier, DSP, the data acquisition system and pressure transducers are located externally in an equipment support box beneath the glove.

A Prandtl probe, which is used to obtain the free stream velocity is mounted below the glove.



Fig. 2 Sailplane Grob G103 Twin II with the glove

Additionally, a thermocouple and a manometer are used to measure the air temperature and absolute pressure, respectively. These parameters are continuously recorded to obtain the free stream boundary conditions. The experiments were carried out at flight velocities from 21m/s to 23m/s. This represents chord Reynolds numbers from $1.8 \cdot 10^6$ to $2.1 \cdot 10^6$.

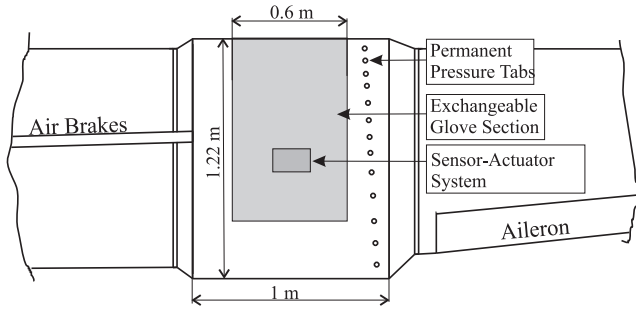


Fig. 3 Sketch of the laminar wing glove

The sensor-actuator system [3] for active wave control consisted of spanwise rows of surface hot-wire reference sensors, a membrane actuator and a spanwise arrangement of hot-wire error sensors. For the initial experiment only one of the sensor-actuator systems was activated.

3.1 Active Control Algorithm

The flow chart of the active wave control algorithm that was used is shown in Fig.4. The reference sensor upstream of the actuator measures the oncoming TS-instabilities (x). The actuator signal (y) is calculated directly from this signal by a convolution with the primary FIR-filter (finite impulse response, FIR_A). The primary transfer function is continuously adapted in order to minimize the error signal (e) measured downstream of the actuator. The path between the actuator and error sensor has to be adapted beforehand in a pre-adaptation calculation. This secondary path (FIR_C) emulates the actuator behaviour and wave superimposition between the actuator and the error sensor.

The primary FIR-filter is continuously changed following the steepest descent of the quadratic error signal (e^2). The gradient method used for the filter update is based on the least

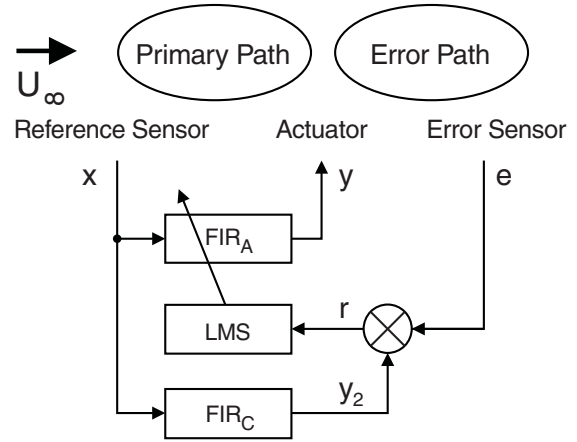


Fig. 4 Filtered-x-LMS algorithm

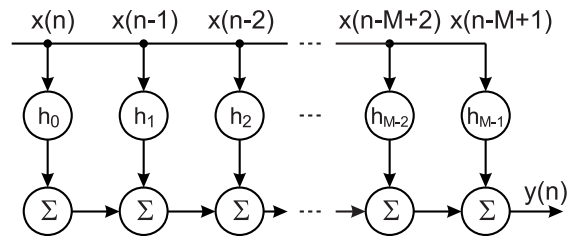


Fig. 5 Transfer function (FIR filter)

mean square (LMS) algorithm. The modified filtered-x-LMS algorithm procedure considers the secondary path to derive a filtered reference signal (y_2). A correlated error signal (r) is derived from the filtered reference and error signal that is applied to perform the LMS-algorithm.

The internal transfer function (FIR filter) that is used is a digital filter which is linear and non recursive. The output signal is the continuously calculated dot product of the continuously shifting input signal and the filter coefficients. The FIR filter is able to precisely model the frequency selective amplification and convection of TS-instabilities. The FIR filter is described as follows:

$$y(n) = \sum_{i=0}^{M-1} h_i \cdot x(n-i)$$

The coefficients of the transfer function are shown in Fig.5.

A digital signal processor (DSP, dspace DS 1103) was employed to achieve a real-time performance of the control algorithm. This processor has direct access to a 16-channel A/D con-

verter with a sampling rate of 1MHz and an 8-channel D/A converter. The analogue input and output channels have a resolution of 16-bits.

3.2 Surface Hot-Wire Sensor

A principle sketch of the surface hot-wire sensor is shown in Fig.6. A platinum-coated tungsten wire ($5\mu\text{m}$ thick) is fixed over a narrow slot (0.075mm - 0.1mm) flush to the surface. For the sensor substrate, a flexible circuit board with a copper layer is used. The slot is easily shaped in the copper layer using the photo-etching technique.

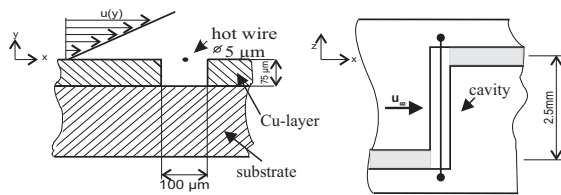


Fig. 6 Sketch of the surface hot-wire sensor

This arrangement produces reduced heat-flux in the structure. Therefore, a higher signal-to-noise ratio is achieved (compared to conventional hot-film sensor arrays) [16]. Modularly arranged hotwire anemometers were designed especially for in-flight measurements to be able to operate a high number of surface hot-wire sensors during flight in constant-temperature mode. The highly sensitive wall sensor was developed especially for measuring the weakest wall shear stress fluctuations. Therefore, this sensor can also be used for measuring the laminar turbulent transition.

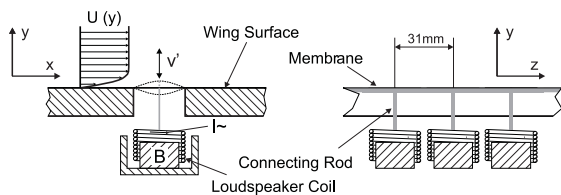


Fig. 7 Sketch of the membrane actuator

3.3 Membrane Actuator

An actuator capable of generating a proper counter wave in the frequency range of the TS-instabilities with a minimal time delay is needed.

The response of the actuator should be linear. Therefore, the membrane actuator was used (Fig.7). The flush-mounted membrane of the actuator was stretched over a spanwise slot of 3mm, which was 25% of the averaged TS-wave length. A connecting rod was fixed between the membrane and the surfaces of the speakers. The modified speakers were used to move the connecting rod and the membrane respectively. A highly elastic membrane material was used to allow sufficient surface displacement with a relatively short membrane length in the streamwise direction. The distance from the surface of the membrane to the bottom of the speaker was approximately 15mm. An exploded view of the used actuator is shown in Fig.8.

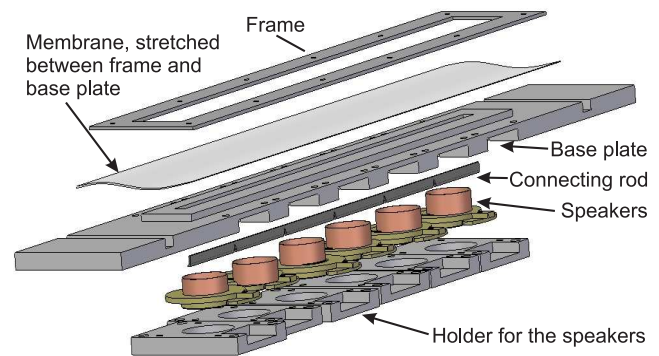


Fig. 8 Sketch of the membrane actuator

The actuator was tested in preliminary measurements. Therefore, the actuator was driven by a signal generator that induced a sinusoidal sweep. The response of the actuator was measured with a laser vibrometer. Fig.9 shows the phase response of the actuator used in accordance to the frequency. The resonance frequency of the actuator is 890Hz and for a frequency of about 500Hz, a 0.15ms time delay (t_a) of the actuator can be detected. For higher frequencies the actuator reaction time rises significantly. At approximately 800Hz a reaction time of about 0.7ms can be expected.

3.4 Boundary Layer Characteristics of the Glove

The performance of the control system strongly depends on the actuator performance, the posi-

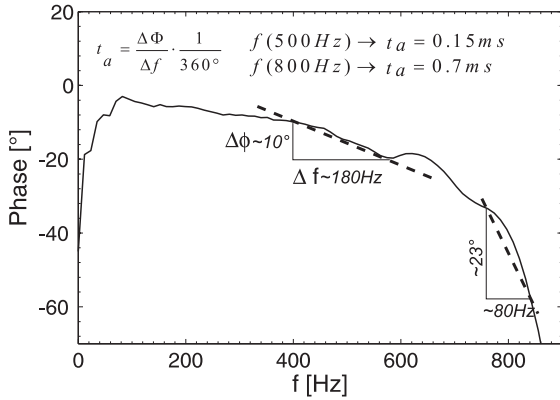


Fig. 9 Phase response of the actuator

tions of the actuators and sensors along the chord as well as the distance between the sensors and the actuator. Therefore in earlier measurements the amplification and transition region were measured on the glove as shown in Fig.10. A piezofoil sensor array was used for these basic in-flight experiments. The sensor and sensor setup are described in [13] and will not be discussed here. The measured amplification rates are essential for the development of the sensor-actuator arrangement for active wave control. The maximum RMS-value marks the maximum amplification of the TS-wave and therefore indicates the transition position. Furthermore, it is evident that transition shifts downstream with a higher flight velocity, because of the lower angle of attack of the sailplane. By viewing the 50% chord length position it is apparent that the maximum amplification occurs for the lowest flight velocity of 21.6m/s. Since the active wave control algorithm can dampen instabilities only in linear amplification stage, the actuator has to be placed before 50% chord length. Besides the detection of the transition position, the harmonic TS-frequencies were detected in a range of about 400Hz to 1000Hz in the basic experiments.

3.5 Sensor-Actuator Setup

The minimum distance between the reference sensor and actuator is dependent on the actuator reaction time and the upstream effects of the actuation. To position the error sensor properly it must be recognized that the generated ac-

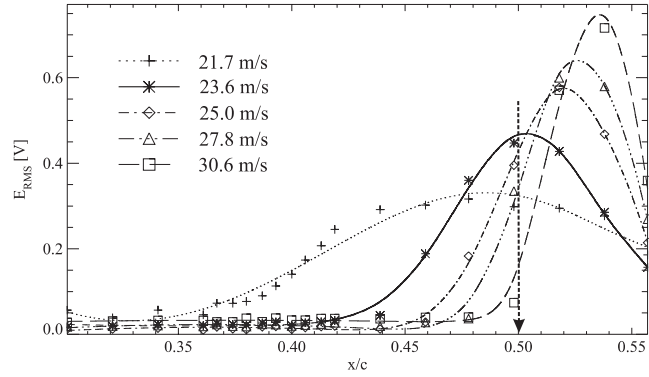


Fig. 10 RMS-values of the disturbance fluctuations on the glove

tuator signal needs at least one TS-wavelength ($\approx 14\text{mm}$) in the streamwise direction to couple in the boundary layer and ultimately affect the instabilities. In regard to the discussed facts, several positions for the reference and error sensor were tested. Additionally, at the chosen chord length position, a spanwise row of sensors were arranged parallel to the actuator. The sketch of the sensor and actuator positions is shown in Fig.11.

The spanwise centerline of the actuator was placed at 47% of the chord length. The spanwise distance between the adjacent arrangement of loudspeakers underneath the glove surface was 31mm. Five spanwise sensor rows were subsequently arranged upstream of the actuator at 43.2% to 45% of the chord length as reference sensors. The spanwise distance between the sensors was 31mm which is also the distance be-

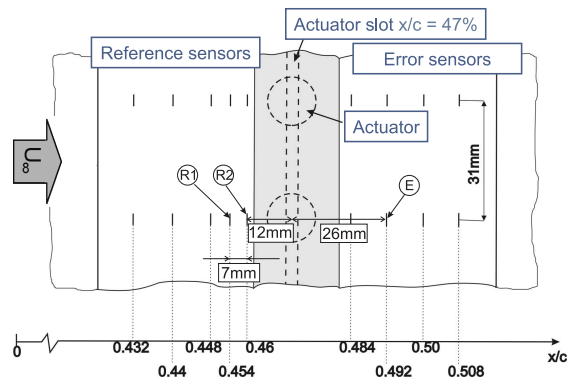


Fig. 11 Positions of reference and error sensors and actuator

tween the speakers. Downstream of the actuator four sensors rows were located at 48.4% to 50.8% as error sensors. During the experiments the most qualified sensors were chosen as reference and error sensors.

4 Results

The boundary layer conditions on the glove for three different flight velocities are documented by means of the frequency spectra of a reference sensor at 46% chord length (Fig.12) and of an error sensor at 49.2% (Fig.13). The spectra of the reference sensors clearly show the amplification of unstable frequencies in the range of 300Hz to 900Hz for all three velocities.

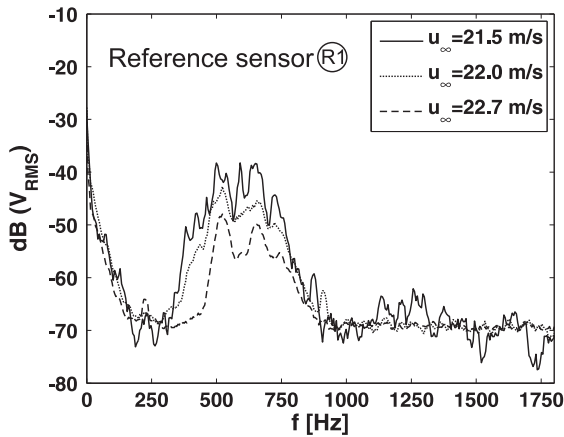


Fig. 12 Spectrum of the reference sensor (R1) at several flight velocities

It is apparent that the amplification of the TS-instabilities decreases with increasing flight velocities, because of the direct connection with flight velocity in gliding flight and angle of attack. The greatest amplification of instabilities occurs at the lowest flight velocity of 21.5m/s at 45.4% chord. Furthermore, initial high harmonic frequencies are also amplified at a velocity of 21.5m/s and a 45.4% streamwise location.

The error sensor located at 49.2% of the chord length (Fig.13) shows that the higher harmonic frequencies are amplified at all velocities, meaning the boundary layer is in its late stage of laminar-turbulent transition. The amplification of the instabilities of the fundamental frequen-

cies has reached saturation. The magnitude of the higher harmonic frequencies indicates different stages of the laminar-turbulent transition.

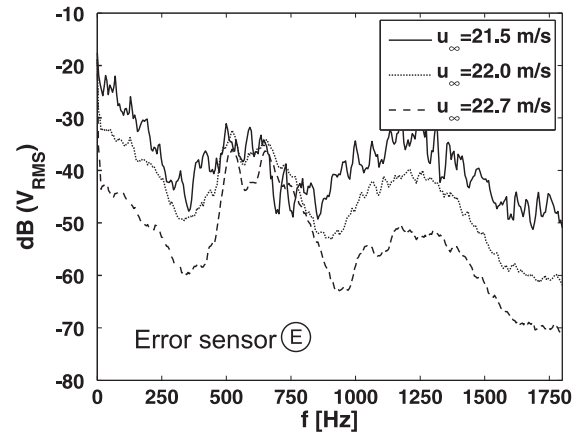


Fig. 13 Spectrum of the error sensor (E) at several flight velocities at natural transition

Fig.14 illustrates the results of the flight measurements with AWC at a flight velocity of 22m/s. The plot depicts time traces of surface hot-wire signals of two reference sensors at 45.5% and 46% of the chord length and an error sensor at 49.2%. Both cases, with and without active wave control (AWC) are shown in addition to the actuator signal, which was calculated and introduced into the boundary layer. Fig.14a depicts the natural, uncontrolled case of the development of TS-instabilities. The reference sensors clearly show the formation of typical TS-wave packets in a very early stage of transition with low amplitudes. It is evident that the amplitude of the error sensor time trace increases considerably without the presence of the actuator signal.

By looking at the time traces of the two reference sensors (R1 and R2) it can be concluded that the phase shift is due to the convective transport process. The actuator signal with AWC (Fig.14b) has a phase shift relative to the reference signal. Comparing the error signals with and without control the reduced amplitude with AWC is noticeable. For Fig.12, only the first reference hot wire sensor (45.4%, R1) and the error sensor at 49.2% (E) were used for the control algorithm.

Fig.15 shows the result of the frequency analysis of the time traces shown in Fig.14a. The

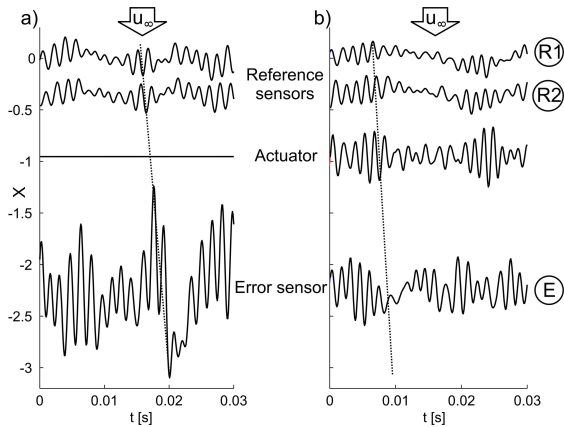


Fig. 14 Time traces of respective reference and error sensors, output signal of the actuator without (a) and with active wave control (b)

spectra of the reference sensors are on the same level; merely the harmonic frequencies of TS-instabilities are amplified. This signifies that both sensors R1 and R2 are in an early amplification stage and are therefore suitable for use as reference sensors in the control system. The frequency spectrum of the error sensor in the case without AWC is also shown in Fig.15. It is apparent that all frequencies are amplified, including the fundamental and first higher harmonics of the unstable TS-frequencies.

Fig.16 illustrates the spectra of the reference and error sensor with and without AWC. The spectrum printed in bold represents the spec-

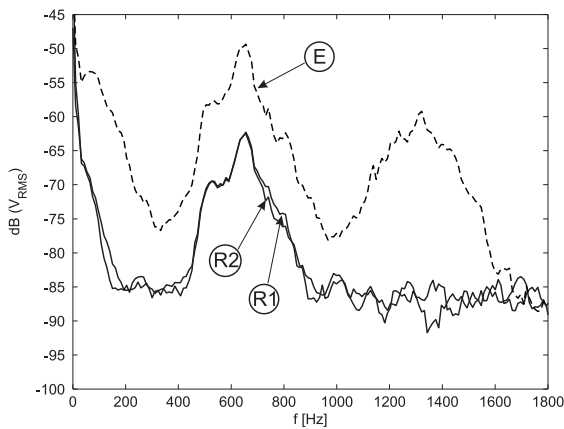


Fig. 15 Comparison of the spectra of the reference and error sensors without AWC ($u_\infty = 22\text{m/s}$)

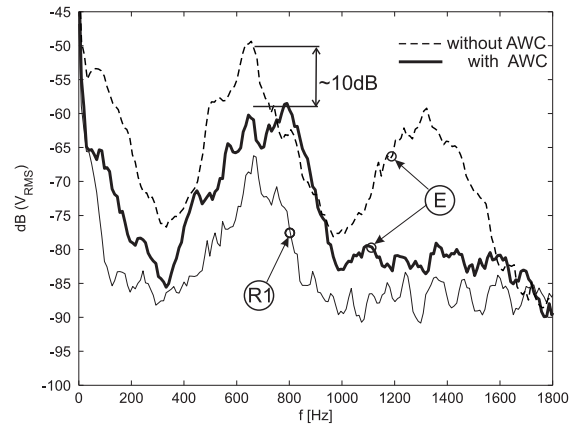


Fig. 16 Spectra of the reference and the error sensor without and with active wave control ($u_\infty = 22\text{m/s}$)

trum of the error sensor with AWC compared to the dashed spectrum of the error sensor without AWC. Comparing these spectra of the error sensor, the lower amplitudes of the instabilities with AWC are noticed. An attenuation of about 10dB is reached, which corresponds to a reduction of the local amplitude by at least 50% and is depicted in Fig.17. Furthermore the higher harmonic instabilities ($f = (1000-1600)\text{Hz}$) are dampened completely. This is due to the direct coupling of the frequency modes.

In spite of this principal success of damping the instabilities, the amplitudes after AWC are still higher than the amplitudes of the instabilities at the reference sensors, meaning the transition can be delayed but the damping rate was not as high as desired. A possible reason could be due to actuator performance. Reviewing the frequency spectra in Fig.16, there is almost no damping in the range of 800Hz to 1000Hz and this could be linked to the actuator resonance frequency. The response time of the actuator increases when approaching the resonance frequency. Therefore the control system will be slow and effectiveness will decrease. It is possible that increasing the distance between the reference sensor and the actuator, the system could improve. Nevertheless, the sensor-actuator control system implemented is the first system which has shown the potential of AWC to delay laminar-turbulent transition

under natural atmospheric conditions in in-flight experiments.

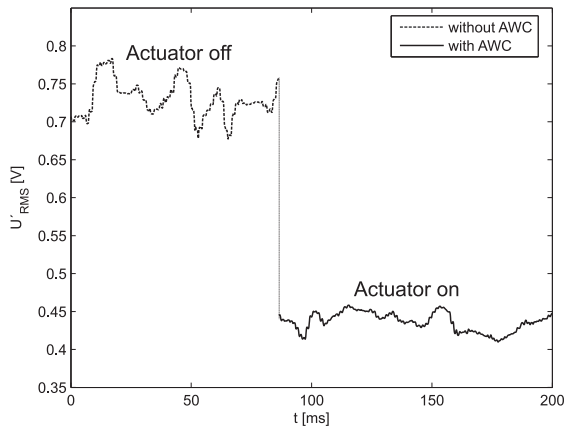


Fig. 17 RMS-values of the error sensor without and with AWC ($u_\infty = 22\text{m/s}$)

5 Conclusion

In-flight experiments of active wave control were carried out with a sailplane on a two-dimensional laminar wing glove. The damping of the natural occurring TS-instabilities by superimposing with a counter wave is the basic idea of the applied control method. Therefore, a sensor-actuator system was developed to measure the oncoming TS-waves and couple the counter wave into the boundary layer. In these experiments a damping of the local amplitudes of the instabilities of about 60% was achieved. The result is relatively small when compared to the wind tunnel experiments, possibly due to poor actuator performance.

This first partial success with AWC-experiments in real atmospheric conditions generates motivation to proceed on this path. An improved actuator with a higher resonance frequency, modified distances between sensors and actuator for more reliable reaction times and an updated control system should improve the entire system and lead to higher damping rates of the instabilities. Besides these modifications, the system will be extended to measure three-dimensional disturbances and control them. Therefore, several sensor-actuator systems working simultaneously will be arranged spanwise

and each single system will be coupled with the adjacent systems. With this coupled system it should be possible to damp three-dimensional and also oblique travelling wave packets, which has already been demonstrated in wind tunnel experiments [17].

Acknowledgements

Special thanks go to a former student and current colleague, Thomas Grund, who worked on these experiments in the framework of his master thesis with enormous dedication.

References

- [1] Abegg C, Bippes H, Boiko A, Krishnan V, Lerche T, Pöthke A, Wu Y, and Dallmann U. Transitional flow physics and flow control for swept wings: Experiments on boundary-layer receptivity, instability excitation and HLF technology. In Thiede P, editor, *Aerodynamic Drag Reduction Technologies*, Vol. 76, pp 199–206, Berlin, Heidelberg, 2001. Springer Verlag.
- [2] Arnal D. Numerical and experimental studies on laminar flow control. *Int. J. for Numerical Methods in Fluids*, Vol. 30, pp 193–204, 1999.
- [3] Baumann M, Sturzebecher D, and Nitsche W. On active control of boundary layer instabilities on a wing. In Nitsche W, Heinemann H.-J, and Hilbig R, editors, *New Results in Numerical and Experimental Fluid Mechanics II*, Vol. 72, pp 22–29, Braunschweig, 1999. Vieweg Verlag.
- [4] Baumann M, Sturzebecher D, and Nitsche W. Active control of TS-instabilities on an unswept wing. In Fasel H and Saric W, editors, *Laminar-Turbulent Transition: IUTAM-Symposium on Laminar-Turbulent Transition 1999 in Sedona USA*, pp 155–160. Springer Verlag, 2000.
- [5] Elliott S. J and Nelson P. A. Active noise control. *IEEE Signal Processing Magazine*, Vol. 10, pp 12–35, 1993.
- [6] Engert M, Pätzold A, and Nitsche W. Development of a sensor-actuator-system for active control of boundary layer instabilities in compressible flows. In Tropea C, Jakirlic S, Heinemann H.-J, Henke R, and Hönlinger H, editors, *Notes on Numerical Fluid Mechanics and Multidisciplinary Design*, Vol. 96, pp 252–259. Springer Verlag, 2007.

- [7] Grundmann S and Tropea C. Active cancellation of artificially introduced Tollmien-Schlichting waves using plasma actuators. *Experiments in Fluids*, Vol. 44, No 5, pp 795–806, Mai 2008.
- [8] Joslin R. Overview of lamina flow control. Technical Report NASA/TP-1998-208705, NASA, Hanover, MD, October 1998.
- [9] Ladd D. M and Hendricks E. W. Active control of 2-d instability waves on an axisymmetric body. *Experiments in Fluids*, Vol. 6, No 1, pp 69–70, Januar 1988.
- [10] Li Y and Gaster M. Active control of boundary layer instabilities. *Journal of Fluid Mechanics*, Vol. 550, pp 185–205, 2006.
- [11] Liepmann H. W, Brown D. L, and Nosenchuck D. M. Control of laminar instability waves using a new technique. *Journal of Fluid Mechanics*, Vol. 118, pp 187–200, 1982.
- [12] Milling R. W. Tollmien-Schlichting wave cancellation. *Physics of Fluids*, Vol. 24, No 5, pp 979–981, 1981.
- [13] Peltzer I. Comparative in-flight and wind tunnel investigation of the development of natural and controlled disturbances in the laminar boundary layer of an airfoil. *Experiments in Fluids*, Vol. 44, No 6, pp 961–972, June 2008.
- [14] Pupator P and Saric W. Control of random disturbances in a boundary layer. Technical Report AIAA Paper 89-1007, AIAA, 1989.
- [15] Saric W. S, Reed H. L, and Kerschen E. J. Boundary layer receptivity to freestream disturbances. *Annu. Rev. Fluid Mech.*, Vol. 34, pp 291–319, 2002.
- [16] Sturzebecher D, Anders S, and Nitsche W. The surface hot wire as a means of measuring mean and fluctuating wall shear stresses. *Experiments in Fluids*, Vol. 31, No 3, pp 294–301, 2001.
- [17] Sturzebecher D and Nitsche W. Active cancellation of Tollmien-Schlichting instabilities on a wing using multi-channel sensor actuator systems. *Int. J. of Heat and Fluid Flow*, Vol. 24, pp 572–583, 2003.
- [18] Thomas A. S. W. The control of boundary-layer transition using a wave superposition principle. *Journal of Fluid Mechanics*, Vol. 137, pp 233–250, 1983.

Copyright Statement

The authors confirm that they, and/or their company or institution, hold copyright on all of the original material included in their paper. They also confirm they have obtained permission, from the copyright holder of any third party material included in their paper, to publish it as part of their paper. The authors grant full permission for the publication and distribution of their paper as part of the ICAS2008 proceedings or as individual off-prints from the proceedings.